

Supplementary information for
“Thermodynamic insights into strong
metal-support interaction of transition metal
nanoparticles on titania: simple descriptors for
complex chemistry”

Xing Wang,^{†,‡} Arik Beck,^{†,‡} Jeroen A. van Bokhoven,^{†,‡} and Dennis Palagin^{*,†,‡}

[†]*Institute for Chemical and Bioengineering, ETH Zurich, Vladimir Prelog Weg 1, 8093
Zurich, Switzerland*

[‡]*Laboratory for Catalysis and Sustainable Chemistry, Paul Scherrer Institute,
Forschungsstrasse 111, 5232 Villigen, Switzerland*

E-mail: dennis.palagin@chem.ethz.ch

S1. Comparison for DFT+U method

In order to study the influence of DFT+U method on the properties of TiO_x monolayers, a U value of 3.0 eV was used to describe the Ti 3d electrons. Table S1 shows the relative stability and Bader charge transfer of TiO_x monolayers supported on Pt (111) with and without DFT+U method. The changes of relative stability and Bader charge transfer for all the monolayers are smaller than 0.1 eV and 0.1 |e| respectively, which indicates that DFT + U value only has only a minor effect on the energy and charge transfer.

Table S1: Influence of DFT+U method. Relative stability (ΔG , eV per TiO_x formula) of TiO_2 , Ti_2O_3 and TiO monolayers supported on Pt (111). Bader charge transfer (ΔQ , |e| per TiO_x formula) from TiO_2 , Ti_2O_3 and TiO monolayers to different metal surfaces. The most stable interface models for the TiO_x are used.

| U value (eV) | ΔG | | ΔQ | |
|-------------------------|---------------|------------|---------------|------------|
| | without DFT+U | with DFT+U | without DFT+U | with DFT+U |
| TiO_2 | 0.38 | 0.46 | 0.02 | 0.01 |
| Ti_2O_3 | -0.79 | -0.81 | -0.49 | -0.54 |
| TiO | -1.10 | -1.19 | -0.53 | -0.60 |

S2. Properties of metal substrates

Table S2: Metal bulk Lattice constants and surface energies of their (111) plane.

| Metal | Lattice constant (\AA) | Surface energy (111) (J/m^2) |
|-------|-----------------------------------|---|
| Cu | 3.612 | 1.44 |
| Ru | 3.768 | 2.91 |
| Rh | 3.812 | 2.02 |
| Pd | 3.924 | 1.38 |
| Ag | 4.114 | 0.82 |
| Os | 3.800 | 3.26 |
| Ir | 3.830 | 2.11 |
| Pt | 3.926 | 1.27 |
| Au | 4.160 | 0.72 |

S3. Relative stability energies

Table S3: Relative stability of anatase-TiO₂ monolayer with different interface models.

| | 1×5 | 1×4 | 2×4 |
|----|--------------|--------------|--------------|
| Cu | 0.26 | 0.3 | 0.46 |
| Ru | 0.13 | 0.08 | 0.39 |
| Rh | 0.25 | 0.23 | 0.43 |
| Pd | 0.49 | 0.31 | 0.31 |
| Ag | 0.73 | 0.62 | 0.32 |
| Os | 0.21 | 0.16 | 0.40 |
| Ir | 0.33 | 0.31 | 0.47 |
| Pt | 0.56 | 0.38 | 0.38 |
| Au | 0.78 | 0.67 | 0.40 |

Table S4: Relative stability of rutile-TiO₂ monolayer in different interface models.

| | 2×6 | 2×5 | 3×5 |
|----|--------------|--------------|--------------|
| Cu | 0.71 | 0.91 | 0.61 |
| Ru | 0.22 | 0.69 | 0.35 |
| Rh | 0.46 | 0.43 | 0.46 |
| Pd | 0.68 | 0.67 | 0.64 |
| Ag | 0.99 | 0.97 | 1.10 |
| Os | 0.29 | 0.81 | 0.31 |
| Ir | 0.52 | 0.44 | 0.49 |
| Pt | 0.67 | 0.73 | 0.64 |
| Au | 1.03 | 0.99 | 1.06 |

Table S5: Relative stability of honeycomb-Ti₂O₃ monolayer in different interface models.

| Metal | 3 × 3 | 4 × 4 | 2 × 2 | 5 × 5 | 4 × 4 | 3 × 3 | 4 × 4 | 5 × 5 | 4 × 4 |
|-------|-------|-----------|-----------|---------|-------|-----------|-----------|-------|-------|
| | 3 × 3 | 5√3 × 5√3 | √19 × √19 | 11 × 11 | 9 × 9 | √31 × √31 | √57 × √57 | 9 × 9 | 7 × 7 |
| Cu | 0.82 | 0.31 | 0.44 | 0.16 | 0.16 | - | - | - | - |
| Ru | 0.08 | -0.46 | -0.55 | -0.44 | -0.4 | - | - | - | - |
| Rh | -0.23 | -0.58 | -0.64 | -0.51 | -0.47 | - | - | - | - |
| Pd | -0.56 | - | - | - | - | - | - | - | - |
| Ag | 0.28 | - | - | - | - | 0.36 | 0.5 | 1.15 | 0.75 |
| Os | -0.12 | -0.65 | -0.49 | -0.52 | -0.49 | - | - | - | - |
| Ir | -0.39 | -0.64 | -0.73 | -0.59 | -0.48 | - | - | - | - |
| Pt | -0.79 | -0.75 | -0.69 | -0.69 | -0.52 | -0.61 | -0.55 | -0.24 | -0.43 |
| Au | 0.01 | - | - | - | - | 0.11 | 0.12 | 0.59 | 0.49 |

S4. Electron density difference and projected density of states

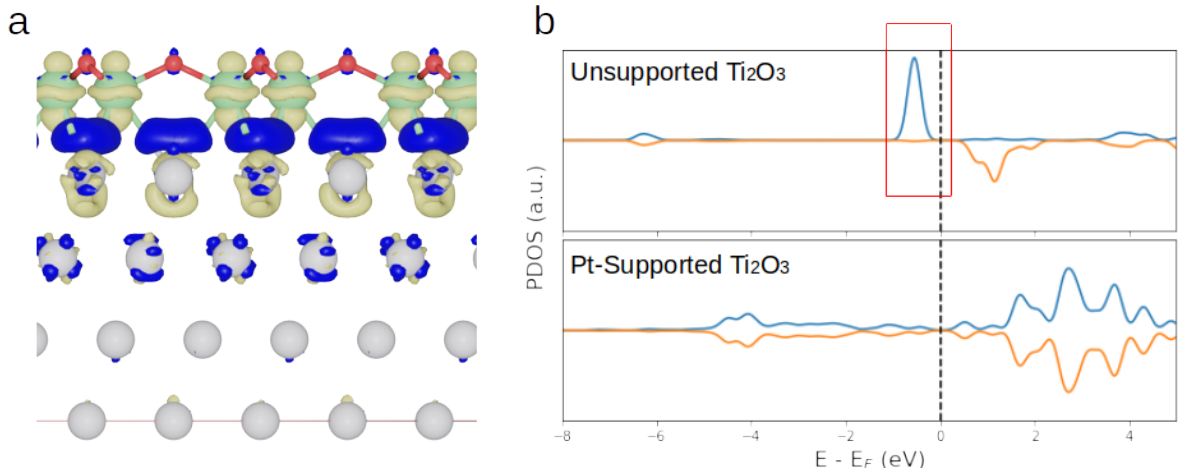


Figure S1: (a) Electron density difference map at the interface between the Ti_2O_3 monolayers and Pt (111) surfaces. The map is defined as the difference between the total electron density of the separated components and that of adsorbed case, while maintaining all the atoms in the positions of the supported configuration. Blue depict the electron excess, and yellow the electron deficit. (b) Projected density of states on Ti cation d_z^2 component in unsupported and Pt (111)-supported Ti_2O_3 honeycomb monolayers respectively. The atomic-like majority peak of d_z^2 character, which is the characteristic of Ti^{3+} in the unsupported monolayer is marked by red rectangle. The vertical dashed lines indicate the position of the Fermi level.

Table S6: Bader charge transfer from TiO_2 , Ti_2O_3 and TiO monolayers to different metal surfaces. A negative value represents charge transfer from monolayer to metal substrate, and a positive value represents the reverse direction.

| Metal | Charge transfer ($ e $ per TiO_x) | | |
|-------|--|-------------------------|--------------|
| | Anatase TiO_2 | Ti_2O_3 | TiO |
| Cu | 0.28 | -0.34 | -0.33 |
| Ru | 0.16 | -0.24 | -0.41 |
| Rh | 0.07 | -0.31 | -0.52 |
| Pd | 0.04 | -0.44 | -0.48 |
| Ag | 0.06 | -0.32 | -0.37 |
| Os | 0.12 | -0.27 | -0.52 |
| Ir | 0.05 | -0.34 | -0.54 |
| Pt | 0.02 | -0.49 | -0.53 |
| Au | 0.02 | -0.40 | -0.51 |

S5. Relative stability of reduced monolayers as a function of surface energy

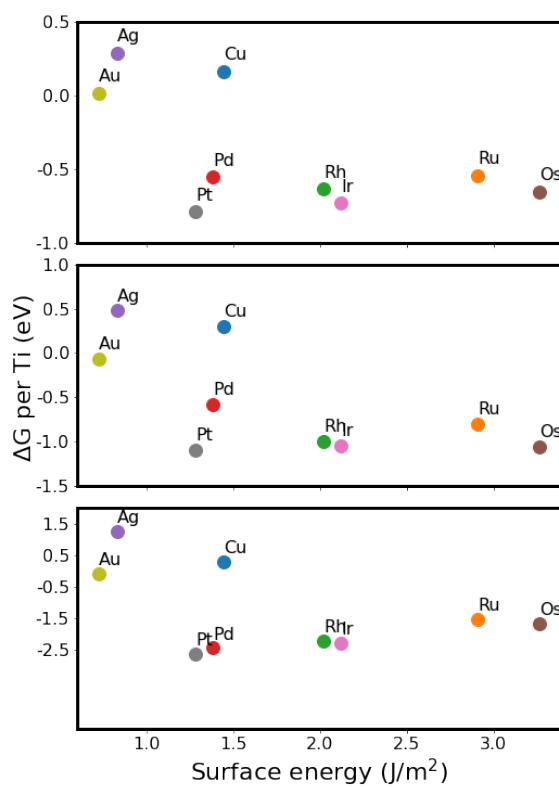


Figure S2: Relative stability of reduced monolayers on metal (111) surfaces as a function of surface energy of the metal substrate.

S6. Descriptor definition

The descriptor for a binary system is defined as the formation energy of the most stable alloy phase, corresponding to this system. For example, Figure S3 demonstrate how this choice is made in the case of Ti–Pt alloy.

Figure S3 shows possible thermodynamically stable alloy phases of the Ti–Pt system, according to the data found in the Materials Project database.¹ In this case, the most negative formation energy (corresponding to the Ti_3Pt_5 phase) should be used as the descriptor for Ti–Pt system. In order to maintain consistency within our work, we calculated the descriptor using our own computational setup and all obtained values are shown in Table S7.

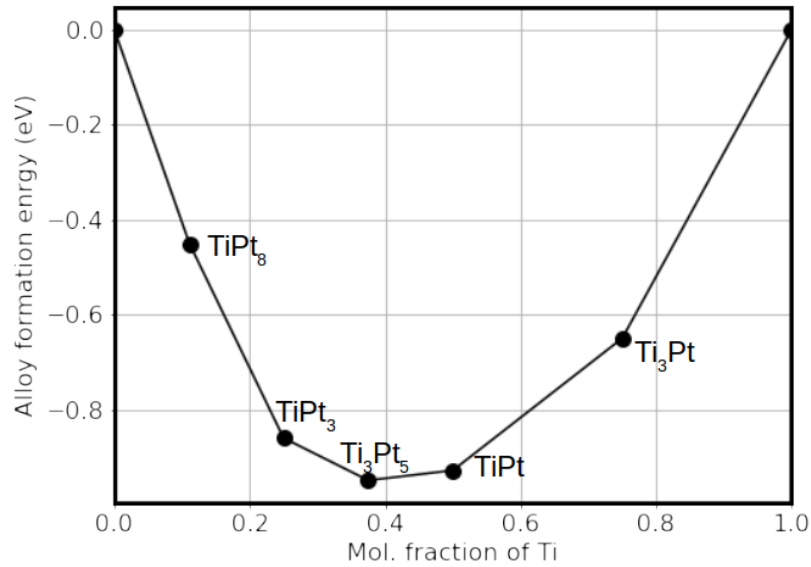


Figure S3: Illustration of the definition of descriptor in the Ti–Pt binary system. Black circles indicate the compositions and formation energies of the thermodynamically stable Ti–Pt phases, as found in the Materials Project database.¹

Table S7: The most stable alloys in the Ti-Me binary systems and their formation energies. Structures are taken from database of Materials Project¹

| System | Alloy | Formation energy (eV/atom) |
|--------|---------------------------------|----------------------------|
| Ti-Cu | TiCu | -0.14 |
| Ti-Ru | TiRu | -0.77 |
| Ti-Rh | Ti ₃ Rh ₅ | -0.81 |
| Ti-Pd | TiPd ₃ | -0.64 |
| Ti-Ag | TiAg | -0.04 |
| Ti-Os | TiOs | -0.71 |
| Ti-Ir | TiIr | -0.87 |
| Ti-Pt | Ti ₃ Pt ₅ | -0.98 |
| Ti-Au | TiAu | -0.42 |

The descriptor for the (Pt–Ag)–Ti ternary system can be calculated by a linear combination of the Pt–Ti and Ag–Ti binary systems:

$$E_{\text{Pt}_x\text{Ag}_{(1-x)}\text{-Ti}} = x \times E_{\text{Pt-Ti}} + (1 - x) \times E_{\text{Ag-Ti}} \quad (\text{S1})$$

S7. Descriptor validation

In order to validate the performance of the descriptor, TiO_x monolayers on a set of alloy systems (Pt–Ag, Cu–Ag and Pt–Ir) are calculated. Table S8 shows the possible alloy phases for the three systems. The structure of the alloy phases include: $R\bar{3}m$, $Pm\bar{3}m$, $P6_3/mmc$, $I4/mmm$. Similar to HCP and FCC structure, all those structures have the same structure for their closest package surfaces. Table S8 shows the relative stability of TiO_x monolayers supported on alloys with $Pm\bar{3}m$ structure and the original structures. The energy differences are smaller than 0.15 eV. Therefore $Pm\bar{3}m$ structure are used for all the alloys for the following validation process.

Figure S4 shows descriptor predicted relative stability for TiO_x monolayers versus the value calculated by DFT. For Ti_2O_3 monolayer, we observed a R^2 of 0.93 and a root mean square error (RMSE) of 0.13 eV. For TiO monolayer, we observed a R^2 of 0.96 and a RMSE of 0.13 eV.

Table S8: Possible structures for Pt-Ag, Cu-Ag and Pt-Ir systems. For the same alloy formula, only the most stable atomic structure is considered.

| System | Formula | Spacegroup | $\Delta G \text{ Ti}_2\text{O}_3$ | | $\Delta G \text{ TiO}$ | |
|--------|------------------------|--------------|-----------------------------------|--------------|------------------------|--------------|
| | | | Original | $Pm\bar{3}m$ | Original | $Pm\bar{3}m$ |
| Ag–Pt | AgPt_4 | $R\bar{3}m$ | | | | |
| | AgPt | $R\bar{3}m$ | –0.10 | –0.16 | –0.28 | –0.32 |
| | Ag_3Pt | $Pm\bar{3}m$ | | | | |
| Ir–Pt | AgPt_3 | $Pm\bar{3}m$ | | | | |
| | IrPt | $R\bar{3}m$ | –0.64 | –0.67 | –1.12 | –1.10 |
| Cu–Ag | IrPt_3 | $Pm\bar{3}m$ | | | | |
| | CuAg_3 | $P6_3/mmc$ | 0.24 | 0.25 | 0.45 | 0.47 |
| | Cu_3Ag | $I4/mmm$ | 0.54 | 0.40 | 0.23 | 0.22 |

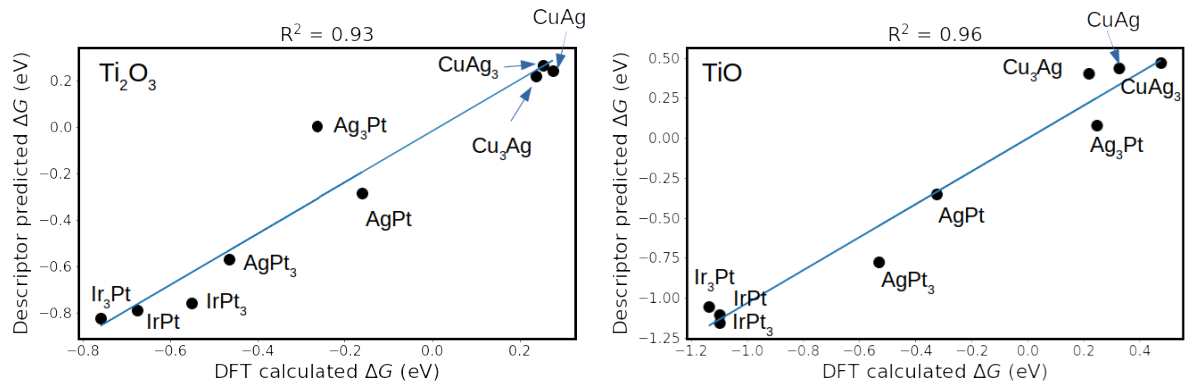


Figure S4: Plot of the descriptor predicted relative stability energies for TiO_x monolayers on a set of alloy substrates with $\text{Pm}\bar{3}m$ structure, versus the value calculated by DFT. Also reported are the correlation coefficient values R^2 . Right: Ti_2O_3 . Left: TiO .

S8. Phase diagrams

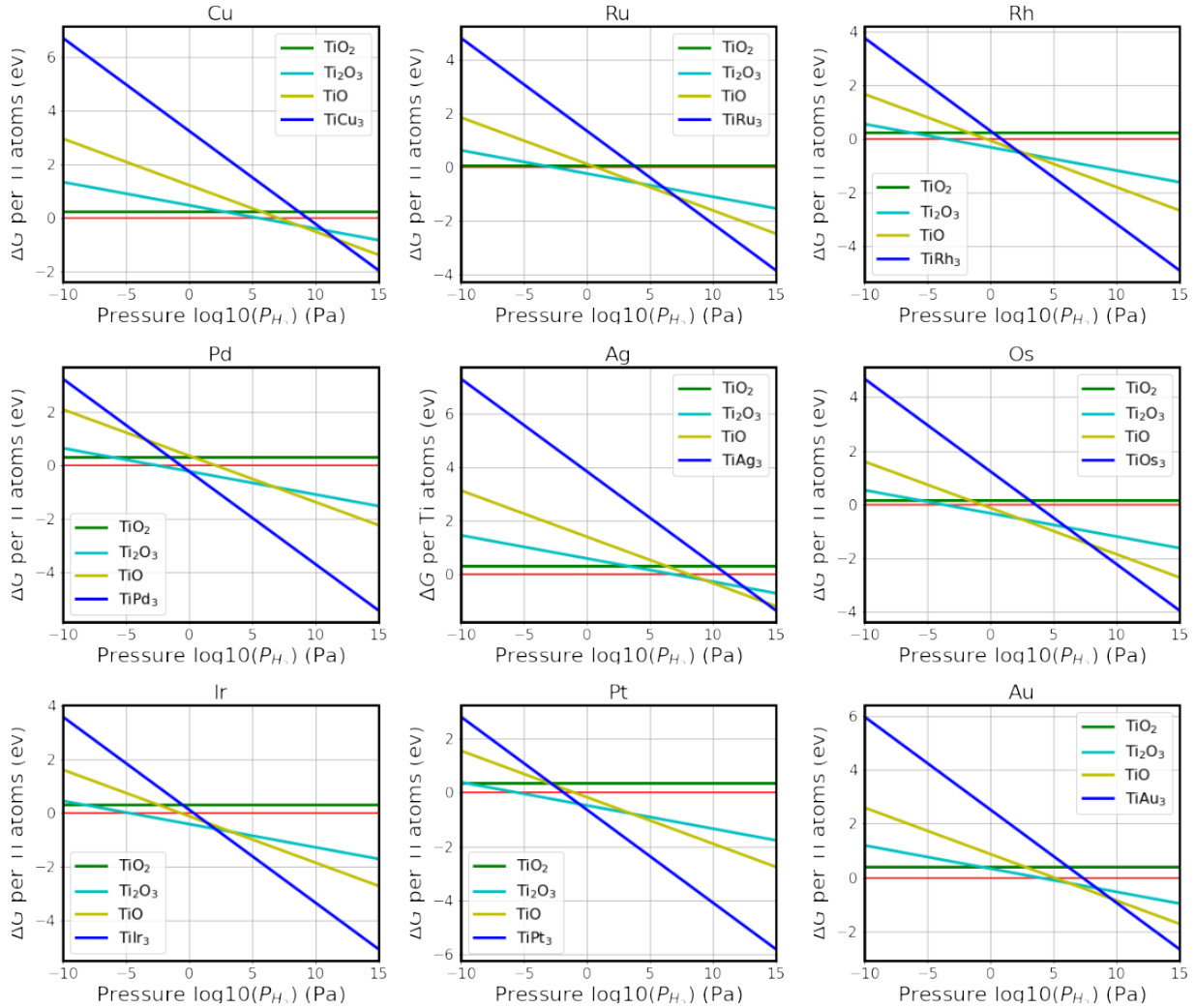


Figure S5: Calculated Gibbs free energy for different TiO_x monolayers on a range of Me(111) surfaces (Me = Pt, Pd, Ru, Ir, Rh, Os, Au, Ag, Cu) as a function of hydrogen pressure at 600 °C. Red line is the reference state of a clean surface without any monolayer. Partial pressure of H_2O is fixed to be 10^{-1} Pa. The stability of reduced monolayers increase with the increasing pressure of hydrogen with different slopes, because the monolayers have different stoichiometry.

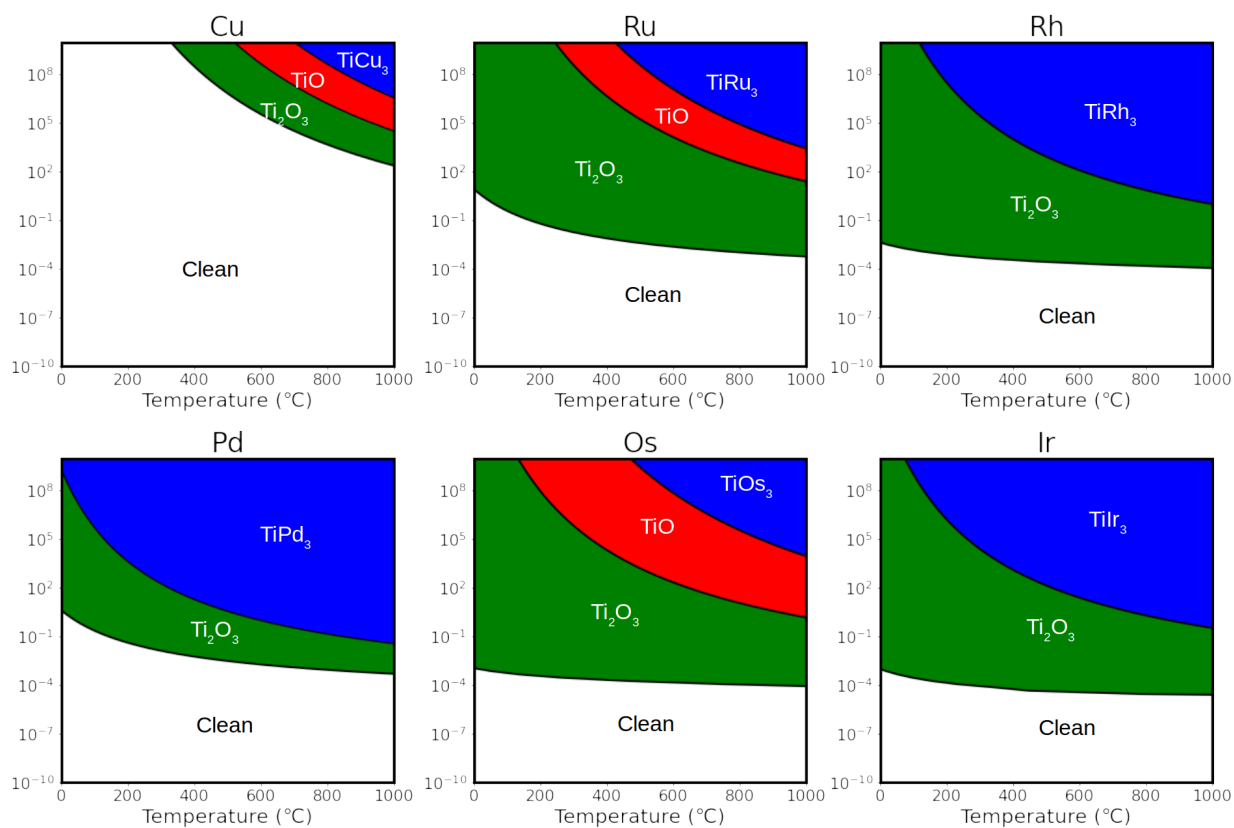
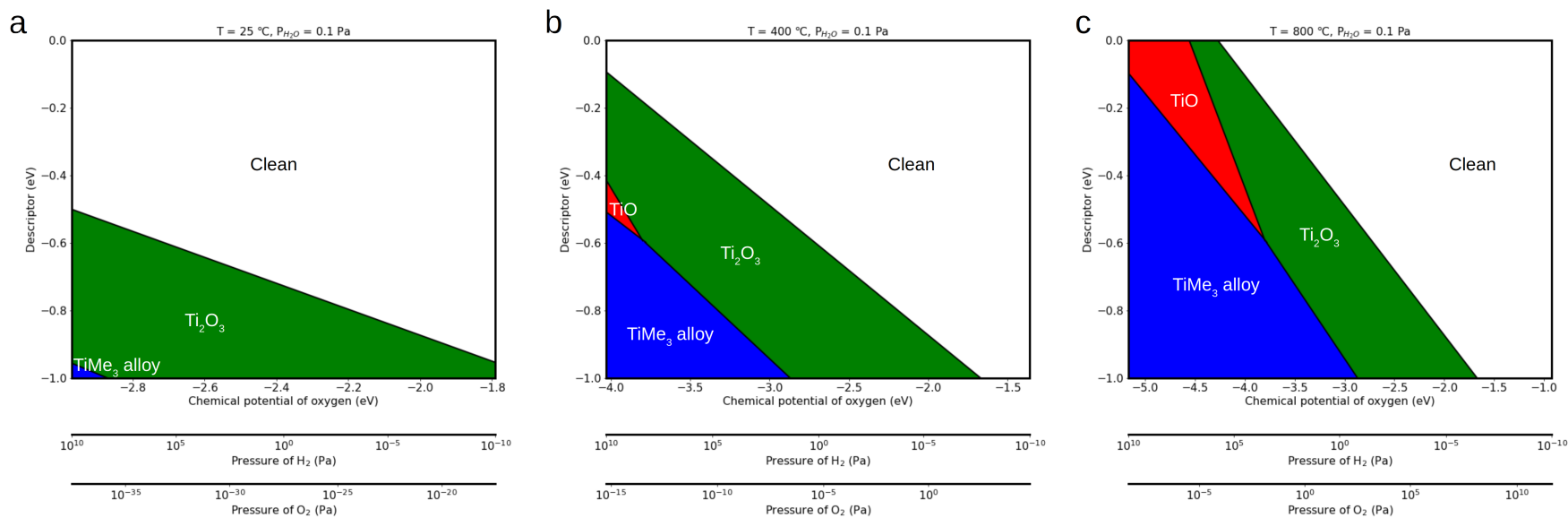


Figure S6: Thermodynamic phase diagrams showing the preferred TiO_x monolayers on metal (Cu, Ru, Rh, Pd, Os, Ir) surfaces as a function of temperature and H_2 pressure. Partial pressure of H_2O is fixed to be 10^{-1} Pa.



14

Figure S7: Phase diagrams showing the preferred monolayers on metal (111) surfaces as a function of the external environmental conditions and the descriptor at different temperature. (a) 25 °C; (b) 400 °C; (c) 800 °C. Conversion between the chemical potential of oxygen and the pressure of hydrogen is done by assuming an equilibrium in the following reaction: $\text{H}_2 + \text{O}_2 \rightleftharpoons \text{H}_2\text{O}$. Partial pressure of H₂O is fixed to be 10⁻¹ Pa.

References

- (1) Jain, A.; Ong, S. P.; Hautier, G.; Chen, W.; Richards, W. D.; Dacek, S.; Cholia, S.; Gunter, D.; Skinner, D.; Ceder, G.; Persson, K. A. The Materials Project: A materials genome approach to accelerating materials innovation. *APL Mat.* **2013**, *1*, 011002.